Analyst

ROYAL SOCIETY OF CHEMISTRY

PAPER

View Article Online
View Journal | View Issue

Cite this: *Analyst*, 2020, **145**, 7907

Evaluating biochemical differences in thyroglobulin from normal and goiter tissues by infrared spectral imaging

Thiago Martini Pereira, *[a,b] Max Diem,[c] Luciano Bachmann,[d] Benjamin Bird,[c,e] Milos Miljković[c,f] and Denise Maria Zezell [b]

Thyroglobulin is a glycoiodoprotein that is produced by thyroid follicular cells; it is stored in follicles in structures known as colloids. The main function of this protein is to stock the hormones triiodothyronine (T3) and thyroxine (T4) until the body requires them. This study aims to demonstrate that infrared spectral imaging with appropriate multivariate analysis can reveal biochemical changes in this glycoprotein. The results achieved herein point out biochemical differences in the colloid samples obtained from normal and goiter patients including glycosylation and changes in the secondary conformational structure. We have presented the first spectral histopathology-based method to detect biochemical differences in thyroid colloids, such as TG iodination, glycosylation, and changes in the secondary structure in normal and goiter patients. The observed changes in the colloids were mainly due to the alterations in amide I and amide II (secondary conformation of proteins) and there is a correlation with different glycosylation between normal and goiter tissues.

Received 8th April 2020,
Accepted 21st August 2020

DOI: 10.1039/d0an00700e

rsc.li/analyst

1. Introduction

The thyroid gland is one of the largest glands of the human endocrine system. This gland secretes mainly the hormones triiodothyronine (T3) and thyroxine (T4), which are required for many physiological processes in the body.[1] The anatomy of thyroid can be described as hundreds of thousands of follicles. Each of these follicles consists of a thin layer of epithelial cells (follicular cells) that produce a protein known as thyroglobulin (TG).[2] Inside of follicles, the colloids are formed in the lumen of the follicles and composed mainly of TG in colloidal form. Its main function is storage of TG, produced by follicular cells, until they are needed by the body.

TG is an iodoglycoprotein and is the major component of the gland. TG comprises a large dimeric glycoprotein (2 × 330 kDa) that contains about 10% of carbohydrates mostly because of glycosylation. This post-transcriptional modification can occur in the rough endoplasmic reticulum and/or the Golgi apparatus.

The synthesis of hormones T3 and T4 is a complex process, and TG plays an important role in their synthesis. Basically, the process can be divided into four steps: TG synthesis, glycosylation, iodination, and coupling. The two first steps take place in the follicular cells, while TG iodination and coupling occur inside the thyroid follicle.

Abnormal TG production leads to abnormal levels of thyroid hormones in the bloodstream, which can indicate goiter.[3,4] The goiter disease refers to an enlargement of the thyroid and can be classified as benign.[5] In the past, the main reason for goiter problems was related to iodine deficiency, so several countries adopted salt iodinization programs to reduce the incidence of this condition worldwide.[6]

Goiter diagnosis starts by evaluating the blood levels of hormones produced by the gland. If abnormal levels are detected, fine needle aspiration biopsy (FNA) guided by ultrasound is performed on the patient.[7] However, in some cases FNA does

[a]*Instituto de Ciência e Tecnologia, Universidade Federal de São Paulo, Rua Talim, 330-12231-280 – São José dos Campos, Brazil. E-mail: t.pereira@unifesp.br; Tel: +55 11 5576-4848, ext 9733*
[b]*Centro de Lasers e Aplicacões, Instituto de Pesquisas Energeticas e Nucleares, Avenida Professor Lineu Prestes 2242, 05508-000 – Sao Paulo, SP, Brazil. E-mail: zezell@usp.br; Tel: +55 11 3133-9370*
[c]*Laboratory for Spectral Diagnosis (LSpD), Department of Chemistry and Chemical Biology, Northeastern University, 360 Huntington Avenue, Boston, USA. E-mail: m.diem@neu.edu; Tel: +1(617)373-5099*
[d]*Universidade de São Paulo, Faculdade de Filosofia Ciências e Letras de Ribeirão Preto, Avenida dos Bandeirantes, 3900 14040-901 Ribeirão Preto, Brazil. E-mail: L.B@usp.br; Tel: +55 16 3315-0366*
[e]*Daylight Solutions, 15378 Avenue of Science, Suite 200, San Diego, CA 92128-3407, USA*
[f]*Department of Mechanical Engineering, Tufts University, 200 Boston Avenue, Medford, Massachusetts 02155, USA*

not provide conclusive pathological diagnosis. This occurs because FNA aspiration often affords few cells.[8] In these cases, the pathologist has difficulty reaching a diagnosis because morphological alterations in the cells are quite relevant information for correct diagnosis. On various occasions, the aspiration needs a high amount of colloids.

Therefore TG offers biochemical information about the physiological process occurring inside these cells[9] and can be used for diagnosis. TG structural conformation, iodination, and glycosylation provide the pathologist and the endocrinologist with valuable knowledge.

Therefore, developing new supporting technologies that can access the biochemical difference in FNA colloids is crucial.

Countless studies[10–14] have reported that FTIR (Fourier transform infrared) imaging is a very sensitive technique to measure protein properties such as structure, folding, unfolding, and misfolding.[15] Several groups around the world are studying a new histopathological method based on FTIR known as spectral histopathology (SHP).[16–18]

Here, we employ SHP to determine the biochemical and biophysical differences in TG found in thyroid tissue biopsies. We aim to explore biochemical and biophysical differences between normal and goiter tissues and to identify changes that could be assigned to TG.

2. Experimental

2.1. Sample preparation

The normal and goiter thyroid tissue microarrays (TH804 and TH805, TMA, BiomaxUS) were used. Each microarray contained 80 different tissue cores measuring *ca.* 1.5 mm in diameter. The paraffin-embedded tissue sections were microtomed at 5 μm thickness and mounted on low-e microscope slides (Kevley Technologies, Chesterland, OH). The tissues are collected under ethical standards with the donor being informed completely and with their consent.

The microarrays were deparaffinized and dried before FTIR measurement.

The dewaxing process was carried out according to the following steps:

1. The slide was heated at 56 °C for 15 minutes.

2. The slide was immersed three times in xylene, each for 5 minutes.

3. The slide was immersed two times in 100% ethanol, each for one minute.

5. The slide was immersed two times in 95% ethanol, each for one minute.

6. The slide was washed with water to remove ethanol.

7. The slide was dried for 24 hours before starting data collection.

The second sequential cut was stained with haematoxylin and eosin (H&E). The H&E slides were used to localize the anatomical features and to correlate them with the hierarchical cluster analysis (HCA) images.

2.2. Data acquisition

The infrared spectra were collected in the transflection mode with a micro-FTIR (Spectrum 1/Spotlight 400, PerkinElmer, Shelton, CT) that incorporated a 16-element focal plane (FPA) detector system. The size of each HgCdTe detector was 25 × 25 μm, and they were cooled with liquid nitrogen. The infrared maps were sampled using a microscope with an additional magnification (4×), leading to an effective pixel size of 6.25 × 6.25 μm. The images were acquired by moving the samples through the focal point of the infrared microscope. This system measured up to 200 spectra per second. Therefore, a 1 mm^2 area consisted of about 20 800 spectra and required *ca.* 40 min for data acquisition. The signal-to-noise ratio was improved by collecting two interferograms per pixel at 4 cm^{-1} spectral resolution.

The entire instrument and the microscope were purged with dry air to keep the relative humidity constant and below 5%, to eliminate the water vapor contribution to the IR spectra.

2.3. Data processing and analysis

2.3.1. Data pre-processing of individual images. The raw hyperspectral imaging dataset comprised 120 000 spectra. Each dataset contained 1625 absorbance data between 750 and 4000 cm^{-1}. The datasets were imported into the in-house written software in the MATLAB environment. Data pre-processing was performed in the following steps:

1. Remove the baseline offset using low intensity between 1600 and 1750 cm^{-1}.

2. Remove the residual water vapor differences in the dataset using the method proposed by Bruun *et al.*[19]

3. Perform a quality test to remove spectra from regions without tissue (noise dataset).

4. Increase the signal to noise using the noise adjusted principal component (NAPC).

5. The pixels without tissue or/and spectrum with strong artefact effects were removed from the dataset.

6. Conversion of the absorbance spectra dataset to the 2nd derivative using the Savitzky–Golay filter (11 smoothing points, 2^{nd} polynomial order).

7. Region restriction spectra to 778–1800 cm^{-1}. The spectra outside this region were deleted.

8. Elimination of Mie scattering effects using the minimum phase correction.[20]

9. Spectra datasets were vector normalized in two regions (900–1350 cm^{-1} and 1352–1800 cm^{-1}) separately and concatenated into a single vector (spectrum).

After pre-processing all images, each image was visualized and an area of c.a. 1 × 1 mm (20 800 spectra) was selected to perform the hierarchical clustering analysis (HCA).

In the HCA, the Euclidean distance was used to define spectral similarity, and Ward's algorithm was applied for clustering. Only the dataset from 900–1350 cm^{-1} was used in the HCA analysis because it included the greatest differences between the types of thyroid tissue.[21] The HCA images of each

tissue were compared to the H&E image, and the cluster (not related to colloids) was deleted from the dataset. In the results, the black pixels correspond to these deleted pixels. The HCA was performed in this step; we named this HCA-PREP.

2.3.2. Cluster analysis of each colloid image. After each image was pre-processed and the spectra that were not related to colloids were removed, we performed the second step of our analysis. The goal of this second step was to look deeply into the relation of the TG secondary structure. To this end, HCA was conducted in the amide I (1600–1700 cm^{-1}) region by using all the spectra in each separated image (normal or goiter). This analysis was named HCA-Amide I. The mean spectra are shown when the data are grouped into nine clusters. Only the results regarding HCA-Amide I are presented in the results section.

2.3.3. Partial least squares discriminant analysis (PLS) analysis. The PLS model was constructed using the datacube from 900–1800 cm^{-1}. In the model, we used a total of 8000 spectra of which 4000 were from normal colloids (500 per patient selected randomly) and 4000 were from goiter colloids (500 per patient selected randomly). The response variable (Y) was built considering the normal group as one and the goiter group as two.

The PLS-DA model was constructed using 7 latent variables (LV) that represent c.a. 96% of variance explained by the model in the predictor variable (Y). To avoid overfitting, we develop our model using 10 k-fold cross validation that means 90% of dataset were used for calibration and the remaining datasets were used to evaluate the PLS model.

3. Results

3.1. Normal tissue

Fig. 1A shows the dendrogram of the normal tissue by using the spectrum hypercube region between 1600 and 1700 cm^{-1}. Fig. 1B displays the image with nine clusters obtained from HCA-amide I. Fig. 1C illustrates the corresponding H&E image of the same area for comparison.

The dendrogram clearly showed three kinds of colloids, which would be divided into more clusters. However, for three clusters, there was a clear division between the evaluated colloids. The nine-cluster image in Fig. 1B revealed that the light green cluster and the red cluster corresponded to only one colloid, that the dark green cluster and the cyan cluster referred to two other colloids, that the white cluster was related to another colloid, and that another set of colloids was defined by three colors: red/brown, grey, and blue.

Fig. 2 illustrates the mean spectra obtained from the nine-cluster spectral image (Fig. 1B). The spectral pattern of the amide I region (which is highly sensitive to the protein secondary structure) clearly corresponded to a mix of α-helix (1655 cm^{-1}) and β-sheet (1694 cm^{-1} and 1628 cm^{-1}) conformations. Intensity differences in the amide II region were small, but the intensity ratio of 1544/1514 changed among the clusters. In the carbohydrate regions, strong peaks centered at 1076 and 1034 cm^{-1} appeared.

3.2. Goiter

Fig. 3 contains the results for one goiter tissue sample. Fig. 3A shows the dendrogram for nine clusters. Comparison with the nine clusters in Fig. 3B revealed some spectral similarity among the different clusters. Considering an image with fewer than nine clusters (not shown), the white and the cyan clusters had characteristics of the same colloid; the similarity between the red and the light green clusters demonstrated another set of colloids. As for the grey and the blue clusters, they corresponded to yet another set of colloids, and the remaining white cluster referred to the last colloid. This analysis pointed out the spectral similarity within the colloid and the spectral differences among neighboring colloids. Fig. 3C shows the H&E image of the same area of a subsequent cut from the same sample.

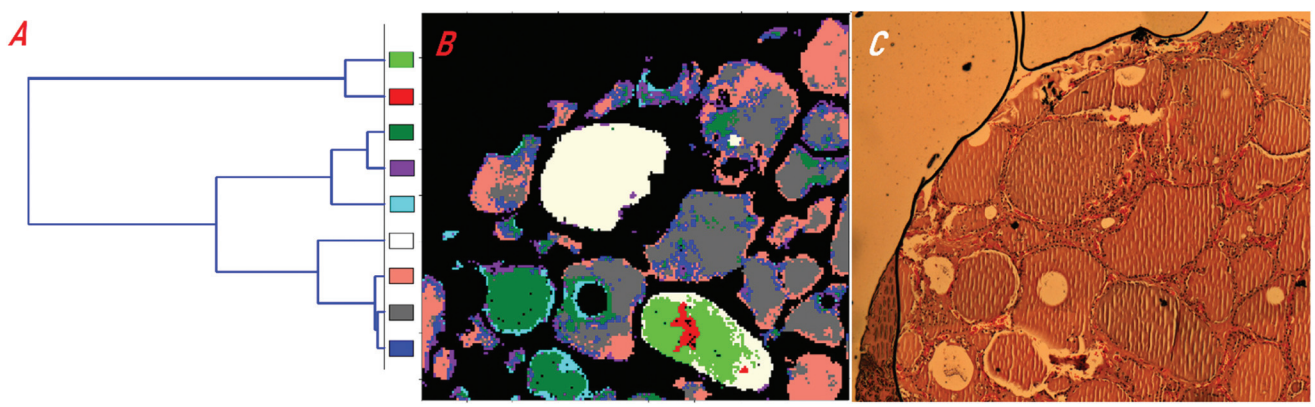

Fig. 1 (A) Dendogram of a normal tissue illustrated in (B) with nine clusters obtained from HCA-amide I; (C) sample stained with H&E for comparison.

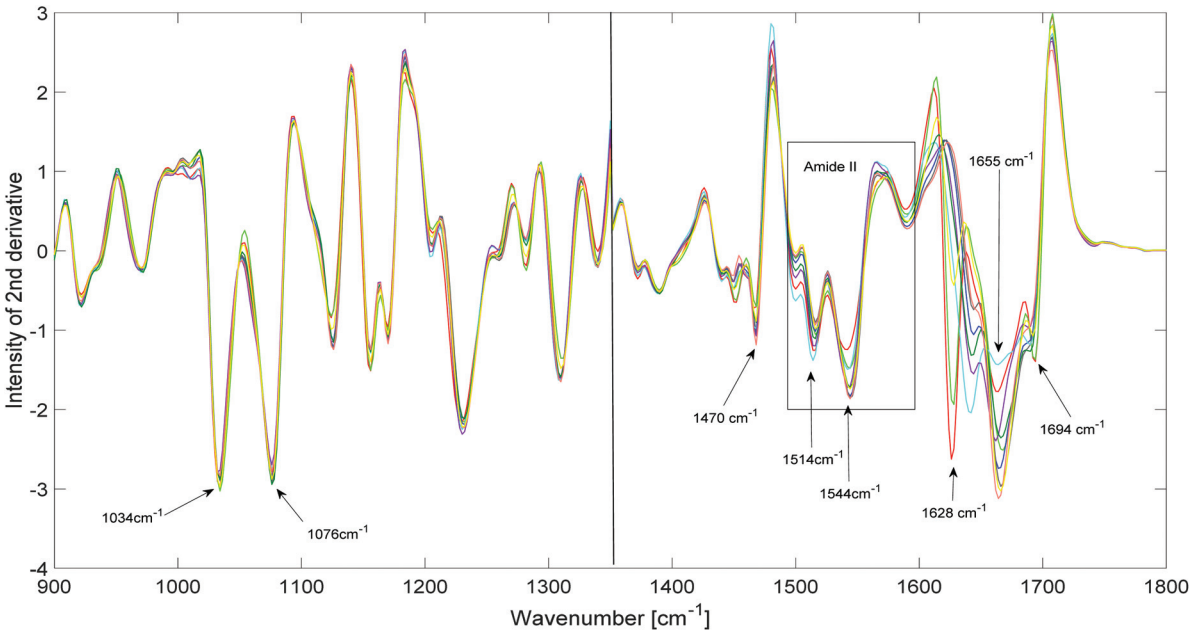

Fig. 2 HCA centroids from the image shown in Fig. 1B.

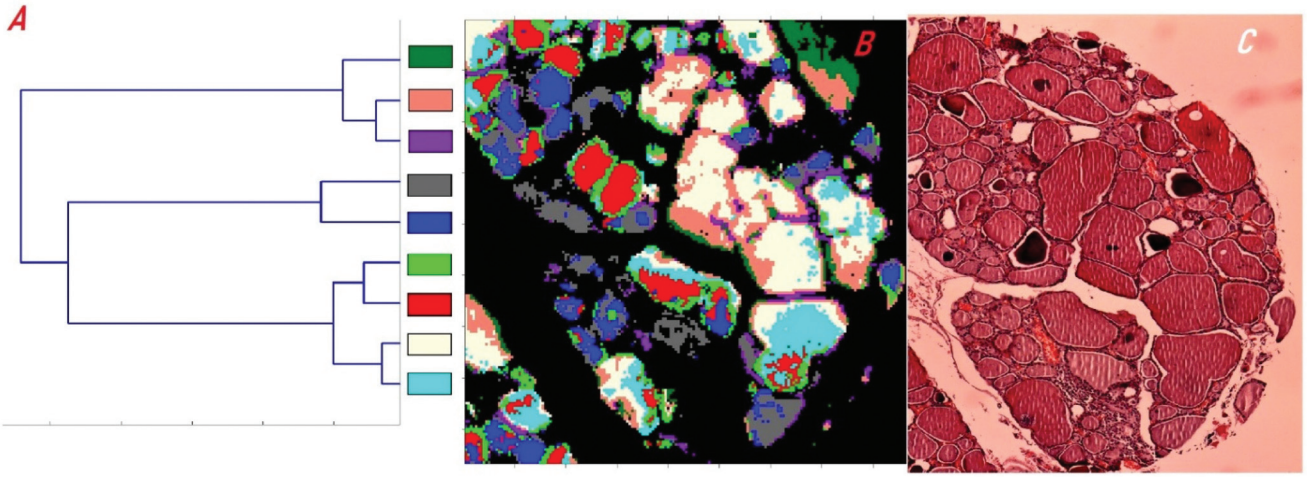

Fig. 3 (A) Dendogram of the goiter tissue and (B) nine-cluster spectral image constructed *via* HCA of the same dataset. (C) H&E image.

Fig. 4 depicts the mean of the second derivative spectra of the nine-cluster HCA (Fig. 3B). A strong peak at 1468 cm^{-1} in some mean cluster spectra revealed a mix of α-helix and β-sheet conformations. On the other hand, the pattern of the mean spectra for the purple spectrum was totally different from the pattern of the normal tissue in the amide I region.

Fig. 5 shows the mean spectra of all the normal tissue samples (total of eight samples). Remember that only the spectra of the colloids were employed.

All the normal tissue samples displayed a strong peak at 1468 cm^{-1}, which was directly linked to the amount of diiodotyrosine (DIT).

As for amide I, the spectra exhibited peaks related to α-helix (1662 cm^{-1}) and β-sheet (1642 cm^{-1} and 1692 cm^{-1}) conformations.

In the amide I region (1600–1700 cm^{-1}), the pattern differed in terms of standard deviation between the normal and the goiter tissues.

The peak at 1662 cm^{-1}, in the carbohydrate region (1030–1074 cm^{-1}), had higher standard deviation for the goiter tissue as compared to the normal tissue.

3.3. PLS analysis

Fig. 6 shows the score plots from the PLS analysis. PC1 divided the normal tissue from the goiter tissue quite well, while PC2 and PC3 were related to spectral differences in each group.

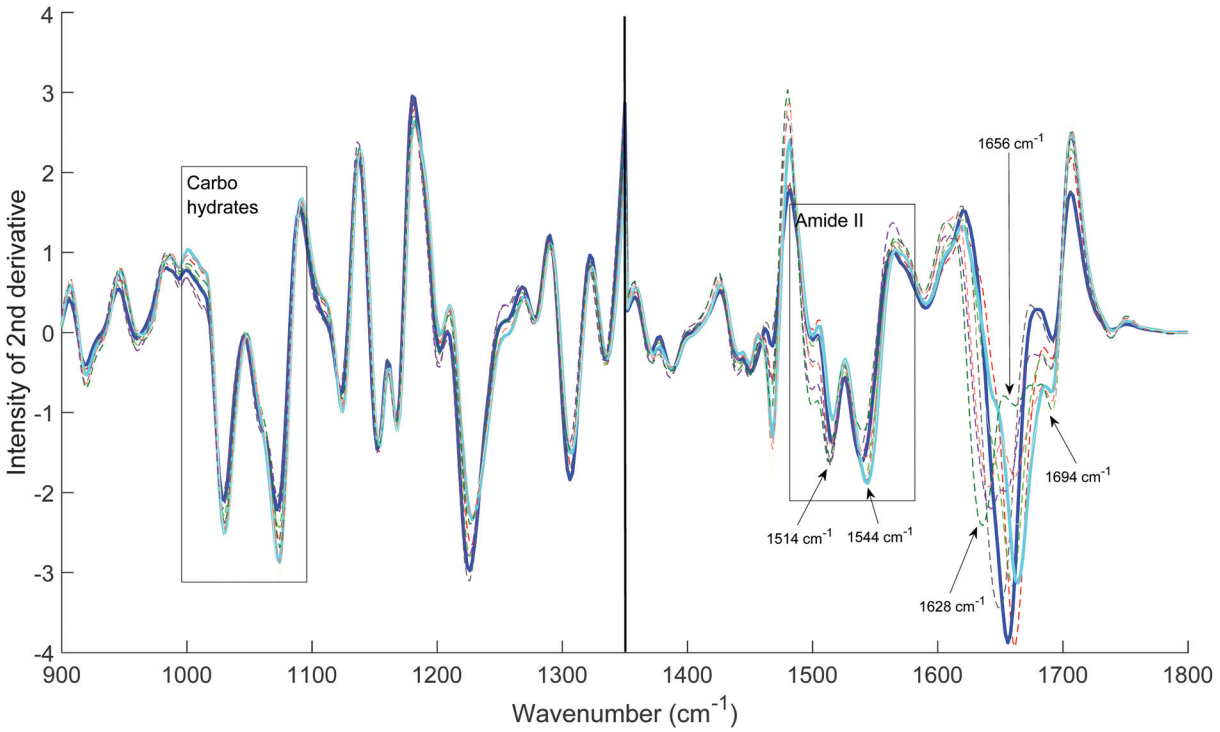

Fig. 4 Mean of the 2nd derivative spectra of the clusters in Fig. 3B. The inset rectangles show the region for amide II and carbohydrate bands.

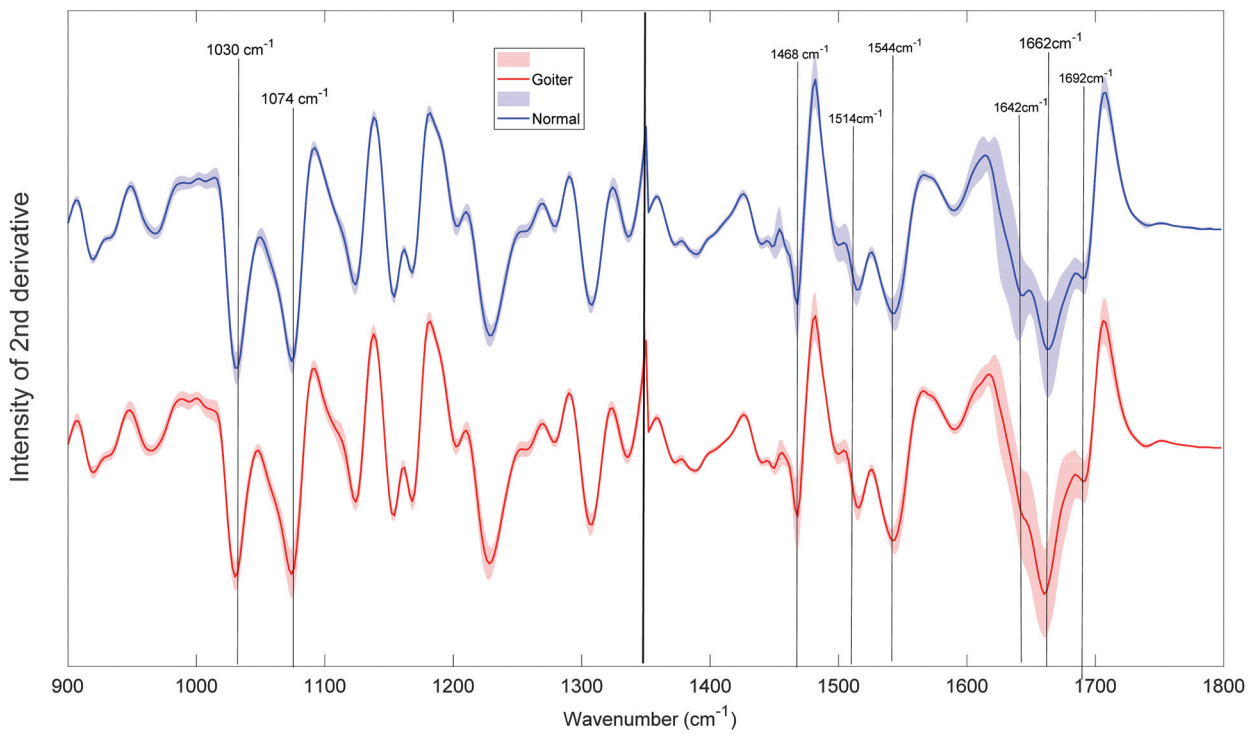

Fig. 5 The 2nd derivative of the mean spectra and standard deviation for the normal (blue) and the goiter (red) tissues.

Fig. 7 contains the loading plot for better visualization of the spectral differences. When we performed the PLS analysis on the second derivative spectra, the maximum value of the loading plot in Fig. 7 corresponded to a minimum value of the corresponding score plot in Fig. 6 and *vice versa*.[22]

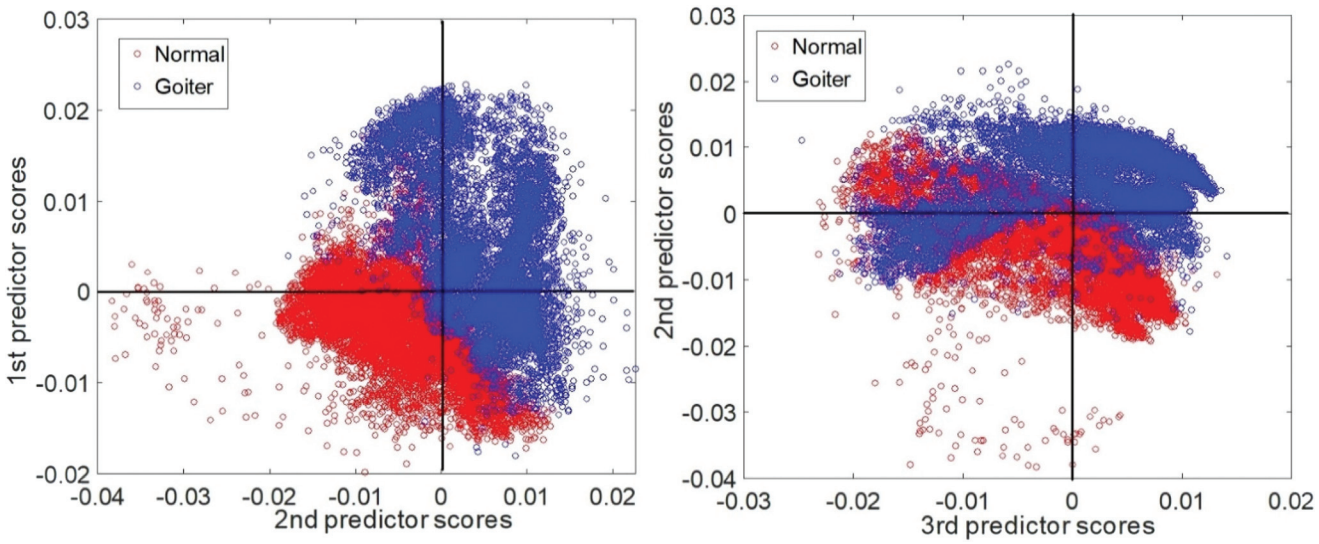

Fig. 6 (A) Shows the score plot 1st predictor score *vs.* 2nd predictor score and (B) brings the score plot 2st predictor score *vs.* 3nd predictor score employing all the data sets for the normal and the goiter samples.

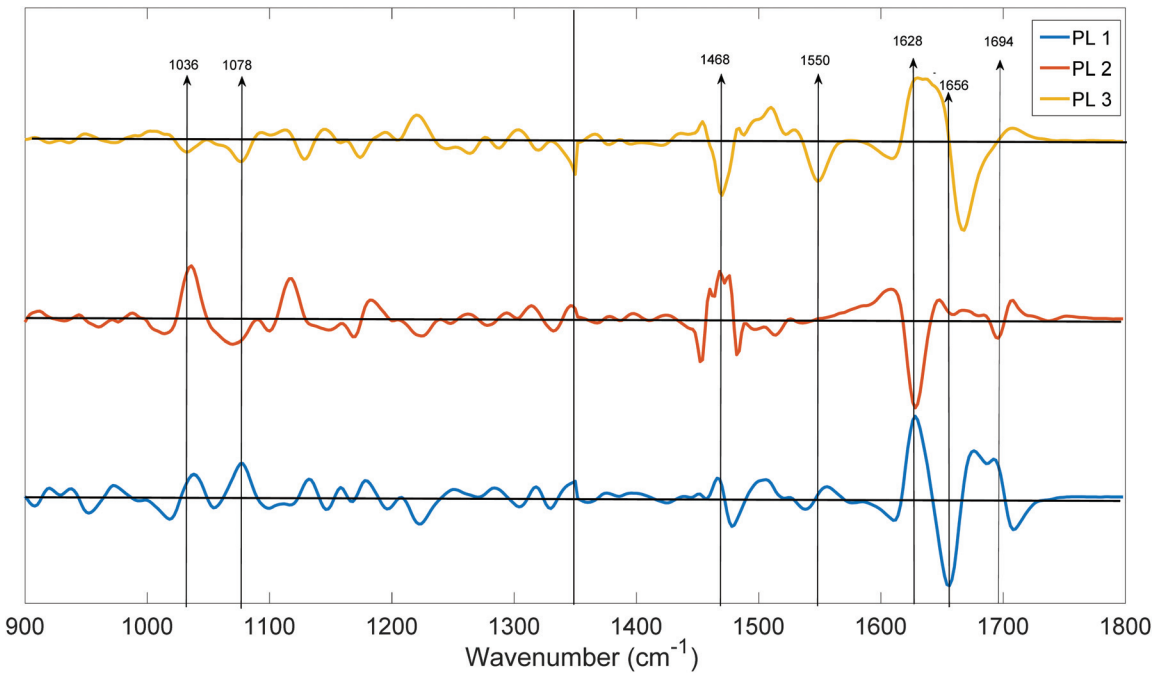

Fig. 7 The 1st, 2nd, and 3rd predictor loading (PL) plots from PLS analysis constructed by using the dataset between 900 and 1800 cm^{-1}. The vertical arrow indicates the position of the main absorption bands.

The PC1 loading revealed differences between the tissues. The main differences lay in the amide I (1600–1700 cm^{-1}) region and in the carbohydrate region (1000–1100 cm^{-1}). The positive peaks at 1036 and 1078 cm^{-1} indicated that these peaks were more intense for the normal tissue than for the goiter tissue. In the PC1 loading plot, the amide I region showed only intensity differences for the peaks at 1628 and 1694 cm^{-1} (β-sheet conformation). These peaks had opposite signals as compared to the peak centered at 1656 cm^{-1} (α-helix conformation).

The PC2 and PC3 loadings pointed out intragroup variance mainly. For the amide I region, PC2 demonstrated pure β-sheet contribution, whereas PC3 showed that the α-helix peak at 1656 cm^{-1} shifted significantly. The peak at 1468 cm^{-1} revealed an opposite signal for PC2 and PC3. Therefore, the PC2 loading showed that the peak at 1468 cm^{-1} peak was

inversely related to the β-sheet conformation peaks in the amide I region.

4. Discussion

On the basis of the results, the colloids have very complex spectral signatures. Basically, they consist of TG, whose formation entails a very elaborate process that can be divided into four steps: protein synthesis, glycosylation, iodination, and conjugation.[1,9] The two first steps occur in the follicular cells, while the two last steps take place in the colloids. Several studies[23–25] have demonstrated that TG plays an important role in glycosylation.

Fig. 2 shows the spectral signatures of normal tissue colloids. There is a clear mix of α-helix (peak at 1655 cm^{-1}) and β-sheet (1694–1628 cm^{-1}) conformations. We had also observed this amide I pattern in our previous study,[26] which evaluated the biochemical changes in normal thyroid tissue. There is no agreement about the TG secondary structure. Few studies[27–29] have demonstrated that the TG secondary structure has a poorly iodinated β-sheet part and another part with a high iodine content.

Here, we verified a relationship between this amide I pattern and the peak at 1468 cm^{-1}, too. The intensity of the peak at 1468 cm^{-1} increased the α-helix peak intensity and decreased the peaks related to the β-sheet conformation. The loading plot from PLS analysis also revealed this fact (Fig. 7). The PC2 loading showed that the peak at 1468 cm^{-1} had the same signal as the α-helix and that these peaks and the peaks referring to the β-sheet conformation (1694–1628 cm^{-1}) had opposite signals.

Our previous study[30] had found this pattern, as well, and shown that the peak at 1468 cm^{-1} was directly linked to the DIT amount. DIT^2 is one of the precursors of thyroid hormone, and it is present at amounts around six times higher than thyroid hormones in the TG molecule.[30]

Looking at the amide II region, we expected wider differences in intensity and/or shifts, but this did not happen. Barth *et al.*[15] suggested that the amide II region is more affected by side-chain contribution than the protein secondary conformation. Glycosylation is one of the possible processes underlying the formation of the TG side chain.[28] In terms of spectral signatures, the glycan content can be assessed by using the carbohydrate region (1000–1100 cm^{-1}).[31,32]

When we observed the PC1 loading (Fig. 7) in the glycan region, the peaks at 1038 and 1074 cm^{-1} had the same signal as the peak at 1468 cm^{-1}, so they were linearly related. We believe that the peak centered at 1038 cm^{-1} had a stronger contribution from glycose,[33] whereas the peak at 1074 cm^{-1} had stronger contribution from mannose.[31] Many studies[25,34] have demonstrated that the mannose content in TG causes intensive T4 synthesis, whilst deglycosylation reduces the amount of T4.

In the PC3 loading, the peak at 1550 cm^{-1} had the same signal as the peaks in the glycan regions. The peak at 1550 cm^{-1} is primarily assigned to N–H bending coupled with the C–N stretching vibrational mode. Alteration in this peak could be explained by the TG *N*-glycation process occurring inside follicular cells. Studies have shown that TG bears about 20 putative *N*-glycosylated sites.[24,34,35] *N*-Glycans located in the TG N-terminal domain participate in tyrosine residue iodination and iodotyrosine coupling.

In the carbohydrate region, the standard deviation of the normal tissue colloids (Fig. 5) was much lower as compared to the goiter tissue colloids. In addition, the normal group colloids provided more intense peaks in the glycan region. These findings indicated that the normal tissue colloids underwent a more homogeneous (less variance and high intensity) glycosylation process as compared to goiter tissue colloids.

At this point, we do not have a full biological explanation. The present results and our previous study[30] showed that, for normal thyroid hormone production, TG must have very specific secondary protein conformation, and that *N*-glycosylation is necessary for this specific conformation. These findings corroborated with the findings of Dupuy *et al.*,[23] who demonstrated that specific biochemical reactions have to happen for correct thyroid hormone synthesis to occur.

Before discussing the results concerning the goiter dataset, we must bear in mind that the TG produced by the cell can be stored in the colloids for several months.[1,2] Thus, the goiter tissue may contain some colloids that were generated by follicular cells under normal physiological conditions. This feature can be noted when we look at the standard deviation of each dataset. The standard deviation for the goiter tissue dataset provided higher values as compared to the normal tissue.

Fig. 4 depicts the spectral signatures of the goiter tissue samples. Two distinct patterns emerged, and the other clusters were a mix of these two patterns. The first cluster (cyan) resembled the one observed in the normal tissue dataset, while the blue cluster revealed a totally different spectral signature. The glycan regions (1000–1100 cm^{-1}) showed that the peak intensities were quite lower in the blue cluster as compared to the dark green cluster.

These alterations in the glycan content revealed that the TG in the cyan cluster (which resembled the normal tissue dataset) was heavily glycosylated as compared to the TG in the blue cluster. The ratio 1032/1074 also changed, indicating that the mannose/glycogen contribution to glycosylation was altered.

According to the literature,[25,36] the TG isoforms have distinct glycosylation patterns, and the post-transcription process is necessary in various physiological processes taking place inside the thyroid follicle, such as TG transport, protein folding iodination, and hormone synthesis.

The differences found in the glycan regions were strictly related to the intensity of the peak at 1468 cm^{-1}. The blue cluster (lower intensity in the glycan regions) did not display this peak, whereas the green cluster had the most intense peak at 1468 cm^{-1}. The latter peak refers to the DIT amount inside a molecule and can indicate the iodine content. According to the literature, thyroid hormones do not occur in unglycosylated isoforms,[34] and the mannose content and the iodine amount in the molecule are correlated.[25]

PLS analysis using all the datasets showed the differences between the normal and the goiter tissue colloids. The score plots (Fig. 6) revealed that PC1 separated normal from goiter tissue colloids quite well. There was a small region in the score plot where normal and goiter tissues were mixed. This result was expected because some colloids in the goiter dataset may have originated in a normal cell condition.[23]

Looking at the loading, PC1 demonstrated significant differences in the intensities of the peaks at 1656, 1628, and 1694 cm^{-1}. This change was mainly due to alterations in the secondary conformation, which can be promoted by processes occurring inside the cell, like glycosylation, as well as processes happening inside the colloid.

The region from 1000 to 1100 cm^{-1} strongly influenced the PC1 score. The observed spectral signatures could be related to glycosylation that is exclusively promoted by follicular cells. This is quite relevant because this kind of information about the colloids can be intrinsically linked to the follicular cells and can be helpful to overcome diagnosis problems that currently exist in the thyroid field. The main reasons for this situation are related to the fact that aspiration from FNA may have few cells for pathological evaluation, so several times the FNA biopsy contains a lot of colloids (TG). In these cases, SHP can be used as an auxiliary tool to aid the pathologist.

PC2 revealed the differences in each dataset, and its loading demonstrated a negative signal at 1468 cm^{-1}, which was opposite to the signal obtained for the peaks at 1636 and 1694 cm^{-1}. These findings showed that, irrespective of tissue type, the iodine amount that is linked to the TG structure is directly and inversely related to the α-helix and β-sheet conformations, respectively.

5. Conclusions

We have presented the first spectral histopathology-based method to detect biochemical differences in thyroid colloids, such as TG iodination, glycosylation, and changes in the secondary structure in normal and goiter patients. Spectral methods can offer this biochemical information fast. The SHP-based method for the analysis of thyroid colloids can help the pathologist to reach more accurate diagnosis.

Conflicts of interest

There are no conflicts to declare.

Acknowledgements

Support for this work from FAPESP 05/51689-2; Instituto Nacional de Fotônica/CNPq 573916/2008-0; CAPES/9036-11-3, CNPq 555621/2009-0 and 308277/2009-0 is gratefully acknowledged. The authors thank Cynthia Maria de Campos Prado Manso for linguistic advice.

References

1 D. Kirsten, *Neonatal Network*, 2000, **19**, 11–26.
2 A. L. Mescher, *Junqueira's basic histology: text and atlas*, Mcgrawhill, United States, 2013.
3 J. C. Moreno and T. J. Visser, *Mol. Cell. Endocrinol.*, 2010, **322**, 91–98.
4 C. Ris-Stalpers and H. Bikker, *Mol. Cell. Endocrinol.*, 2010, **322**, 38–43.
5 L. Hegedüs, S. J. Bonnema and F. N. Bennedbæk, *Endocr. Rev.*, 2003, **24**, 102–132.
6 M. Sanjari, A. Gholamhosseinian, N. Nakhaie, M. Shokoohi and M. Moeini, *J. Kerman Univ. Med. Sci.*, 2010, 226–234.
7 P. Trimboli, N. Nasrollah, L. Guidobaldi, S. Taccogna, D. Domenico, C. Modica, S. Amendola, F. Romanelli, A. Lenzi, G. Nigri, M. Centanni, L. Giovanella, S. Valabrega and A. Crescenzi, *World J. Surg. Oncol.*, 2014, **12**, 61.
8 J. Yang, V. Schnadig, R. Logrono and P. G. Wasserman, *Cancer*, 2007, **111**, 306–315.
9 B. Di Jeso and P. Arvan, *Endocr. Rev.*, 2016, **37**, 2–36.
10 V. Gaydou, M. Polette, C. Gobinet, C. Kileztky, J. F. Angiboust, M. Manfait, P. Birembaut and O. Piot, *Anal. Chem.*, 2016, **88**(17), 8459–8467.
11 P. Bassan, M. J. Weida, J. Rowlette and P. Gardner, *Analyst*, 2014, **139**, 3856–3859.
12 A. Akalin, X. Mu, M. A. Kon, A. Ergin, S. H. Remiszewski, C. M. Thompson, D. J. Raz, M. Diem, B. Bird and M. Miljkovic, *Lab. Invest.*, 2015, **95**, 406–421.
13 F. de Lima and L. Bachmann, *USP*, 2016.
14 M. J. Romeo and M. Diem, *Vib. Spectrosc.*, 2005, **38**, 115–119.
15 A. Barth, *Biochim. Biophys. Acta*, 2007, **1767**, 1073–1101.
16 D. Christensen, A. Rüther, K. Kochan, D. Pérez-guaita and B. Wood, *Annu. Rev. Anal. Chem.*, 2019, 1–20.
17 D. Andrew, D. Perez-Guaita, P. Heraud, J. Beeson, D. Anderson, J. Richards and B. R. Wood, *Faraday Discuss.*, 2016, **187**, 341–352.
18 H. J. Byrne, M. Baranska, G. J. Puppels, N. Stone, B. Wood, K. M. Gough, P. Lasch, P. Heraud, J. Sulé-Suso and G. D. Sockalingum, *Analyst*, 2015, **140**, 2066–2073.
19 S. W. Bruun, A. Kohler, I. Adt, G. D. Sockalingum, M. Manfait and H. Martens, *Appl. Spectrosc.*, 2006, **60**, 1029–1039.
20 M. Miljkovic, B. Bird and M. Diem, *Analyst*, 2012, **137**, 3954–3964.
21 W. Kabbach, D. M. Zezell, M. C. Bandéca, T. M. Pereira and M. F. Andrade, *Laser Phys.*, 2010, **20**, 1833–1837.
22 M. Kozicki, D. J. Creek, A. Sexton, B. J. Morahan, A. Weselucha-Birczynska and B. R. Wood, *Analyst*, 2015, **140**, 2236–2246.
23 D. P. Carvalho and C. Dupuy, *Mol. Cell. Endocrinol.*, 2017, **458**, 6–15.
24 S. X. Yang, H. G. Pollock and A. B. Rawitch, *Arch. Biochem. Biophys.*, 1996, **327**, 61–70.

25 M. Zabczyńska, K. Kozłowska and E. Pocheć, *Int. J. Mol. Sci.*, 2018, **19**, 2792.
26 T. M. Pereira, D. M. Zezell, B. Bird, M. Miljković and M. Diem, *Analyst*, 2013, **138**, 7094–7100.
27 V. Deshpande and S. G. Venkatesh, *Biochim. Biophys. Acta, Protein Struct. Mol. Enzymol.*, 1999, **2**, 157–178.
28 B. Di Jeso and P. Arvan, *Endocr. Rev.*, 2015, **37**, 2–36.
29 S. Formisano, C. Noscatelli, R. Zarrilli, B. Ieso, R. Acquaviva, S. Obici, G. Palumbo and R. Lauro, *Biochem. Biophys. Res. Commun.*, 1985, **133**, 766–772.
30 T. M. Pereira, D. M. Zezell, B. Bird, M. Miljković and M. Diem, *Analyst*, 2013, **138**, 7094–7100.
31 M. Khajehpour, J. L. Dashnau and J. M. Vanderkooi, *Anal. Biochem.*, 2006, **348**, 40–48.
32 A. Travo, O. Piot, R. Wolthuis, C. Gobinet, M. Manfait, J. Bara, M. E. Forgue-Lafitte and P. Jeannesson, *Histopathology*, 2010, **56**, 921–931.
33 M. Diem, A. Mazur, K. Lenau, J. Schubert, B. Bird, M. Miljkovic, C. Krafft and J. Popp, *J. Biophotonics*, 2013, **6**, 855–886.
34 B. Mallet, P. Lejeune, N. Baudry, P. Niccoli and P. Carayon, *J. Biol. Chem.*, 1995, **270**, 29881–29888.
35 N. Baudry, P. J. Lejeune, P. Niccoli, L. Vinet, P. Carayon and B. Mallet, *FEBS Lett.*, 1996, **396**, 223–226.
36 B. Mallet, P. J. Lejeune, N. Baudry, P. Niccoli, P. Carayon and J. L. Franc, *J. Biol. Chem.*, 1995, **270**, 29881–29888.